Synthesis, Structural Characterization (X-ray and EXAFS), and Magnetic Properties of Polynuclear Manganese(II) Complexes with Chlorobenzoato Bridges

Belen Albela,[1a] Montserrat Corbella,*[,1a] Joan Ribas,[1a] Isabel Castro,[1b] Jorunn Sletten,[1c] and Helen Stoeckli-Evans[1d]

Departament de Quimica Inorgànica, Universitat de Barcelona, Diagonal 647, 08028 Barcelona, Spain, Departament de Quimica Inorgànica, Universitat de València, Dr. Moliner 50, 46100 Burjassot (València), Spain, Department of Chemistry, University of Bergen, Allégatan 41, N-5007 Bergen, Norway, and Institut de Chimie, Université de Neuchâtel, Avenue de Bellevaux 51, CH-2000 Neuchâtel, Switzerland

Received July 25, 1997

Three different types of polynuclear Mn^{II} complexes with carboxylate bridges were obtained from the reaction of $Mn(RCOO)_2$ with 2,2′-bipyridine (bpy). Dinuclear complexes $[Mn_2(\mu\text{-}RCOO)_2(bpy)_4](ClO_4)_2$ with R = 2-ClPh, 3-ClPh, 4-ClPh, Ph (**1**−**4**); trinuclear complexes $[Mn_3(\mu\text{-}RCOO)_6(bpy)_2]$ with R = 2-ClPh, 3-ClPh (**5**, **6**), $[Mn_3(\mu\text{-}RCOO)_6(2,2'\text{-}Me_2\text{-}bpy)_2]$ with R = 2-ClPh, 3-ClPh, 4-ClPh (**7**−**9**), and 1D complexes $[Mn(\mu\text{-}RCOO)_2(bpy)]_n$ with R = 3-ClPh, 4-ClPh (**10**, **11**). $[Mn_2(\mu\text{-}PhCOO)_2(bpy)_4](ClO_4)_2$ (**4**) and the $[Mn(\mu\text{-}3\text{-}ClPhCOO)_2(bpy)]_n \cdot nH_2O$ (**10**) have been characterized by X-ray diffraction. Complex **4** crystallizes in the triclinic system, space group $P\bar{1}$ with $a = 9.1886(10)$ Å, $b = 11.6135(9)$ Å, $c = 13.595(2)$ Å, $\alpha = 66.225(13)°$, $\beta = 84.073(12)°$, $\gamma = 88.593(10)°$, $Z = 1$. Complex **10** crystallizes in the monoclinic system, space group $C2/c$ with $a = 26.376(5)$ Å, $b = 12.404(3)$ Å, $c = 7.095(1)$ Å, $\beta = 96.10(3)°$, $Z = 4$. The other complexes were characterized by XANES and EXAFS studies, by comparison with analogous complexes of known X-ray crystal structure. The Mn···Mn distances in the dinuclear complexes and in the infinite chains were similar (*av* 4.5 Å) and longer than for the trinuclear complexes (*av* 3.6 Å); this is in agreement with the number of carboxylate bridges: two in the first case and three for the trinuclear complexes. All the polynuclear complexes shown very weak antiferromagnetic coupling (J between -0.7 and -3.22 cm^{-1}). So, at low temperatures more than one spin state may be populated and many possible transitions may be expected in the EPR spectra; each series shows a similar spectrum, which is different from the others.

Introduction

The manganese(II) carboxylate system is one of the few areas of Mn^{II} chemistry in which a significant amount of structural data is available. Most Mn^{II} carboxylates and their hydrates are stable in air but some of them, for example $[Mn(Bu^tCOO)_2]$, react readily to form red-brown trinuclear Mn^{III} species. Monomers are known—for example, $[Mn(RCOO)(H_2O)_5](RCOO)$; however, most structures involve bridging carboxylates, which can be coordinated to the metals in various fashions,[2] giving rise to polynuclear species. Indeed, as underlined by Wieghardt,[3] carboxylate groups show a pronounced tendency to bind manganese in either a monodentate or a bidentate manner; in the latter case, often with the formation of a symmetrical μ-*syn*-*syn* carboxylate bridge.

In contrast to dimanganese(III) complexes, effective self-assembly routes to carboxylate-bridged dimanganese(II) compounds are limited owing to the lability of Mn^{II} ions and their tendency to undergo both substitution and redox reactions. Structurally characterized examples reported show either only carboxylates or carboxylates and other bridging ligands. These complexes model the bonding characteristics of biomolecules with two neighboring Mn^{II} ions, since polypeptides often have unbound $-COO^-$ groups which can be used in coordination to metal ions. With only carboxylate bridges, there are reports of species that possess only one,[4,5] two,[2,6−9] or three carboxylates[6,10−12] bridging the two Mn^{II} centers. However, a dimeric tetrabridged species with the copper(II) acetate structure has not been reported. Recently, a Mn^{II} dimer bridged by two

(1) (a) Departament de Química Inorgànica. Universitat de Barcelona. (b) Departamento de Química Inorgánica, Universidad de Valencia. (c) Department of Chemistry, University of Bergen. (d) Institut de Chimie, Université de Neuchâtel.

(2) (a) Chiswell, B. In *Comprehensive Coordination Chemistry*; Pergamon: Oxford, 1987; Vol IV, p 43. (b) Rardin, R. L.; Tolman, W. B.; Lippard, S. J. *New J. Chem.* **1991**, *15*, 417.

(3) Wieghardt, K. *Angew. Chem., Int. Ed. Engl.* **1989**, *28*, 1153.

(4) Chen, X. M.; Tang, Y. X.; Xu, Z. J.; Wak, T. C. W. *J. Chem. Soc., Dalton Trans.* **1995**, 4001.

(5) Adams, H.; Bailey, N. A.; Debaecker, N.; Fenton, D. E.; Kanda, W.; Latour, J. M.; Okawa, H.; Sakiyama, H. *Angew. Chem., Int. Ed. Engl.* **1995**, *34*, 2535

(6) Shake, A. R. Ph.D. Thesis, University of Indiana, Bloomington, IN, 1990.

(7) Oshio, 0. H.; Ino, E.; Mogi, I.; Ito,T. *Inorg. Chem.* **1993**, *32*, 5697.

(8) Che, C. M.; Tang, W. T.; Wong, K. Y.; Lai, T. F. *J. Chem. Res., Synop.* **1991**, 30.

(9) Glowiak, T.; Kozlowski, H.; Erre, L. S.; Micera, G. *Inorg. Chim. Acta* **1995**, *236*, 149.

(10) Wieghardt, K.; Bossek, U.; Nuber, B.; Weiss, J.; Bonvoisin, J.; Corbella, M.; Vitols, S. E.; Girerd, J. J. *J. Am. Chem. Soc.* **1988**, *110*, 7398.

(11) Matsushima, H.; Ishiwa, E.; Nakashima, M.; Tokii, T. *Chem. Lett.* **1995**, 129.

(12) Osawa, M.; Singh, U. P.; Tanaka, M.; Morooka,Y.; Kitajima, N. *J. Chem. Soc., Chem. Commun.* **1993**, 310.

S0020-1669(97)00935-X CCC: $15.00
Published on Web 02/04/1998

carboxylate groups was described, in which the dicarboxylate bridge belongs to a single large ligand.[13] In other complexes both metals are bridged not only by carboxylates, but also by other typical ligands such as μ-aqua,[14−16] μ-hydroxo,[17] μ-phenoxo,[18−23] and μ-alcoxo.[24]

On the other hand, the number of trinuclear Mn^{II} complexes with bridging carboxylato groups is limited, and all of them present only these kinds of bridging ligands.[25−30] Finally, although manganese(II)−carboxylate systems are usually polynuclear, few one-dimensional polymers have been described; examples are reported elsewhere.[31−39]

In this paper we report the isolation and characterization of three kinds of Mn^{II} compound of different nuclearity: dinuclear complexes $[Mn_2(\mu\text{-RCOO})_2(bpy)_4](ClO_4)_2$, trinuclear complexes $[Mn_3(\mu\text{-RCOO})_6(bpy)_2]$, and one-dimensional compounds $[Mn(\mu\text{-RCOO})_2(bpy)]_n\cdot nH_2O$. The structural characterization was achieved by X-ray diffraction and EXAFS techniques. The magnetic behavior of these compounds has been studied, as has their EPR spectra.

Experimental Section

Materials. All manipulations were performed under aerobic conditions. Reagent grade solvents were used without further purification. Organic reagents were used as received except 2-ClPhCOOH, 3-ClPhCOOH, and 4-ClPhCOOH, which were recrystallized from hot water. Yield was calculated from the stoichiometric reaction. The $[Mn(RCOO)_2]\cdot nH_2O$ (R = 2-ClPh; 3-ClPh; 4-ClPh, Ph) were synthesized by the reaction of freshly prepared $MnCO_3$ and R-COOH in hot water: after several hours, the solution was filtered and the solvent was reduced by rotatory evaporation, giving a pale pink precipitate of the desired product.

Syntheses. $[Mn_2(\mu\text{-RCOO})_2(bpy)_4](ClO_4)_2$, R = 2-ClPh, 3-ClPh, 4-ClPh, Ph (1−4). $[Mn(RCOO)_2]\cdot nH_2O$ (R = 2-ClPh; 3-ClPh; 4-ClPh, Ph) (1.0 mmol) and $NaClO_4\cdot H_2O$ (0.14 g, 1.0 mmol) were mixed in absolute ethanol (50−100 mL). The resulting mixture was filtered to remove any impurity, and 2,2′-bipyridine (0.30 g; 2.0 mmol) in ethanol (20 mL) was added. The solution turned yellow immediately and was stored at room temperature for several hours. The yellow solid formed was collected by filtration, washed in ethanol and ether, and dried in air. The yield was high (85−90%). For complex **2,** when the filtered solution was left to stand in the open air for several days, a new product was isolated, which did not present the perchlorate anion and corresponded to the chain **(10)**. Complex **3** precipitated only in the presence of excess $NaClO_4$ (2−3 g); however, if the above ratio was used the corresponding chain **(11)** was obtained. Suitable crystals were isolated only for complex **4**, by slow evaporation at room temperature of an EtOH/H_2O (1:1) solution of the initial solid. Anal. Calcd. for complex **1**, $C_{54}H_{40}Cl_4Mn_2N_8O_{12}\cdot 3H_2O$: C, 50.0; H, 3.54; N, 8.62. Found: C, 50.7; H, 3.6; N, 8.4. FT-IR data (KBr, main bands, cm^{-1}): 1600 (vs), 1561 (s), 1474 (m), 1439 (s), 1401 (s), 1144 (m), 1118 (vs), 1088 (vs), 1016 (m), 765 (s), 754 (s), 648 (m), 624 (m). Analysis calculated for complex **2**: $C_{54}H_{40}Cl_4Mn_2N_8O_{12}$: C, 52.09; H, 3.22; N, 9.00; Cl, 11.41. Found: C, 52.2; H, 3.2; N, 8.9; Cl, 11.4. FT-IR data (KBr, main bands, cm^{-1}): 1609 (vs), 1563 (s), 1475 (m), 1439 (s), 1387 (s), 1120 (m), 1089 (vs), 1016 (m), 768 (s), 757 (m), 624 (m). Anal. Calcd for complex **3**, $C_{54}H_{40}Cl_4Mn_2N_8O_{12}$: C, 52.09; H, 3.22; N, 9.00; Cl, 11.41. Found: C, 51.7; H, 3.2; N, 9.0; Cl, 11.4. FT-IR data (KBr, main bands, cm^{-1}): 1608 (vs), 1561 (vs), 1474 (m), 1438 (vs), 1400 (vs), 1147 (m), 1118 (s), 1088 (vs), 1015 (s), 776 (m), 764 (vs), 738 (m), 624 (m), 530 (m). Anal. Calcd for complex **4**, $C_{54}H_{42}Cl_2Mn_2N_8O_{12}$: C, 55.19; H, 3.61; N, 9.54; Cl, 5.96. Found: C, 55.1; H, 3.6; N, 9.4; Cl, 6.0. FT-IR data (KBr, main bands, cm^{-1}): 1602 (vs), 1561 (vs), 1474 (m), 1438 (vs), 1392 (vs), 1118 (s), 1089 (vs), 1016 (s), 766 (s), 714 (m), 625 (m).

$[Mn_3(\mu\text{-RCOO})_6(bpy)_2]$, R = 2-ClPh (5), 3-ClPh (6). 2,2′-Bipyridine (0.16 g, 1.0 mmol) in EtOH (20 mL) was added to a solution of $[Mn(RCOO)_2]\cdot nH_2O$ (0.40 g; 1.0 mmol) in absolute ethanol (30 mL). The resulting mixture was left undisturbed at room temperature for several hours. A yellow microcrystalline powder was formed, which was filtered, washed in ethanol and ether, and air dried. The yield was 70−85%. In the synthesis of complex **6**, upon prolonged storage of the filtrate at room temperature, a second yellow product was isolated, whose analysis again corresponded to the chain **(10)**, which is described below. Anal. Calcd for complex **5**, $C_{62}H_{40}Cl_6Mn_3N_4O_{12}$: C, 52.76; H, 2.83; N, 3.97; Cl, 15.10. Found: C, 52.2; H, 3.0; N, 4.0; Cl, 15.0. FT-IR data (KBr, main bands, cm^{-1}): 1611 (vs), 1570 (s), 1450 (m), 1439 (s), 1387 (vs), 1058 (m), 1118 (vs), 762 (vs), 650 (m). Anal. Calcd for complex **6**, $C_{62}H_{40}Cl_6Mn_3N_4O_{12}$: C, 52.76; H, 2.83; N, 3.97; Cl, 15.10. Found: C, 52.8; H, 2.9; N, 4.0; Cl, 15.1. FT-IR data (KBr, main bands, cm^{-1}): 1611 (vs), 1565 (vs), 1400 (vs), 1156 (m), 1010 (m), 768 (vs), 736 (s), 446 (m).

$[Mn_3(\mu\text{-RCOO})_6(Me_2\text{-bpy})_2]$, R = 2-ClPh (7), 3-ClPh (8), 4-ClPh (9). $[Mn(RCOO)_2]\cdot nH_2O$ (0.50 g, 1.2 mmol) and 4,4′-dimethyl-2,2′-bypiridine (Me_2-bpy) (0.18 g, 1.0 mmol), both dissolved in absolute ethanol, were mixed with constant stirring. The total volume of EtOH used was *ca*. 120 mL. The yellow solid formed was isolated by filtration, washed in ethanol and ether, and dried in air. Yield: 85−95%. Anal. Calcd for complex **7**, $C_{66}H_{48}Cl_6Mn_3N_4O_{12}$: C, 54.02; H, 3.27; N, 3.82; Cl, 14.53. Found: C, 53.9; H, 3.4; N, 3.8; Cl, 14.3. FT-IR data (KBr, main bands, cm^{-1}): 1618 (vs), 1540 (s), 1450 (m), 1407 (vs), 1065 (m), 815 (m), 755 (s), 657 (m). Anal. Calcd for complex **8**, $C_{66}H_{48}Cl_6Mn_3N_4O_{12}$: C, 54.02; H, 3.27; N, 3.82; Cl, 14.53. Found: C, 54.0; H, 3.3; N, 3.7; Cl, 14.1. FT-IR data (KBr, main bands, cm^{-1}): 1611 (vs), 1555 (vs), 1420 (m), 1394 (vs), 834 (m), 762 (s), 700 (m). Anal. Calcd for complex **9**, $C_{66}H_{48}Cl_6Mn_3N_4O_{12}$: C, 54.02; H, 3.27; N, 3.82; Cl, 14.53. Found: C, 53.6; H, 3.4; N, 3.8; Cl, 14.2.

(13) Tanase, T.; Lippard, S. J. *Inorg. Chem*. **1995**, *34*, 4682.
(14) Caneschi, A.; Ferraro, F.; Gatteschi, D.; Melandri, M. C.; Rey, P.; Sessoli, R. *Angew. Chem., Int. Ed. Eng.* **1989**, *28*, 1365.
(15) Yu, B. S.; Lippard, S. J.; Shweky, I.; Bino, A. *Inorg. Chem*. **1992**, *31*, 3502.
(16) Coucouvanis, D.; Reynolds, R. A.; Dunham, W. R. *J. Am. Chem. Soc*. **1995**, *117*, 7570.
(17) Bossek, U.; Wieghardt, K.; Nuber, B.; Weiss, J. *Inorg. Chim. Acta* **1989**, *165*, 123
(18) Gultneh, Y.; Farooq, A.; Liu, S.; Karlin, K. D.; Zubieta, J. *Inorg. Chem*. **1992**, *31*, 3607.
(19) Higuchi, C.; Sakiyava, H.; Okawa, H.; Isobe, R.; Fenton, D. E. *J. Chem. Soc., Dalton Trans.* **1994**, 1097.
(20) Mikuriya, M.; Fujii, T.; Kamisawa,S.; Kawasaki, Y.; Tokki, T.; Oshio, H. *Chem. Lett.* **1990**, 1181.
(21) Sakiyama, H.; Tamaki, H.; Kodera, M.; Matsumoto, N.; Okawa, H. *J. Chem. Soc., Dalton Trans.* **1993**, 591.
(22) Higuchi, C.; Sakiyawa, H.; Osawa, H.; Fenton, D. K. *J. Chem. Soc., Dalton Trans.* **1995**, 4015.
(23) Wada, H.; Motoda, K.; Ohba, M.; Sakiyama, H.; Matsumoto, N.; Okawa, H. *Bull. Chem. Soc. Jpn.* **1995**, *68*, 1105.
(24) Pessiki, P. J.; Khangulov, S. V.; Ho, D. M.; Dismukes, G. C. *J. Am. Chem. Soc*. **1994**, *116*, 891.
(25) Hubner, K.; Roesky, H. W.; Noltemeyer, M.; Bohra, R. *Chem. Ber*. **1991**, *124*, 515.
(26) Menage, S.; Vitols, S. E.: Bergerat, P.; Codjovi, E.; Kahn, O.; Girerd, J. J.; Guillot, M.; Solans, X.; Calvet, T. *Inorg. Chem.* **1991**, *30*, 2666.
(27) Vincent, B.; Christou, G. *Adv. Inorg. Chem. Radiochem*. **1989**, *32*, 197.
(28) Rardin, R. L.; Bino, A.; Poganiuch, P.; Tolman, W. B.; Liu, S.; Lippard, S. J. *Angew. Chem., Int. Ed. Eng.* **1990**, *29*, 812.
(29) Rardin, R. L.; Poganiuch, P.; Bino, A.; Goldberg, D. P.; Tolman, W. B.; Liu, S.; Lippard, S. J. *J. Am. Chem. Soc.* **1992**, *114*, 5240.
(30) Zhong, Z. J.; You, X.-Z.; Mak, T. C. W. *Polyhedron* **1994**, *13*, 2157.
(31) Cano, J.; Munno, D.; Sanz, J.; Ruiz, R.; Lloret, F.; Faus, J.; Julve, M. *J. Chem. Soc., Dalton Trans*. **1994**, 3465.
(32) Wagner, G. R.; Friedberg, S. A. *Phys. Lett*. **1964**, *9*, 11.
(33) Osaki, H.; Nakai, Y.; Watanabe, T. *J. Phys. Soc. Jpn*. **1963**, *18*, 919.
(34) Lis, T. *Acta Crystallogr. A* **1977**, *24*, 348.
(35) Chen, X. M.; Mak, T. C. W. *J. Crystallogr. Spectrosc. Res*. **1991**, *21*, 21.
(36) Chen, X. M.; Mak, T. C. W. *Inorg. Chim. Acta* **1991**, *189*, 3.
(37) Marioni, P.-A.; Marty, W.; Stoeckli-Evans, H.; Whitaker, C. *Inorg. Chim. Acta* **1994**, *219*, 161.
(38) Solans, X.; Gali, S.; Font-Altaba, M.; Oliva, J.; Herrera, J. *Afinidad* **1989**, *45*, 247
(39) Borrás-Almenar; J. J.; Burriel, R.; Coronado, E.; Gatteschi, D.; Gómez-García, C. J.; Zanchini, C. *Inorg. Chem*. **1991**, *30*, 947.

FT-IR data (KBr, main bands, cm^{-1}): 1607 (vs), 1560 (s), 1415 (vs), 1097 (m), 1018 (m), 782 (s), 540 (m).

$[Mn(\mu\text{-}3\text{-}ClPhCOO)_2(bpy)]_n \cdot nH_2O$ (10). A solution of $[Mn(3\text{-}ClPhCOO)_2]\cdot nH_2O$ (0.40 g, 1.0 mmol) in absolute ethanol (50 mL) was treated with 2,2′-bipyridine (0.16 g; 1.0 mmol) in EtOH (50 mL). The resulting yellow solution was left undisturbed for 24 h. The yellow microcrystalline solid formed corresponded to trinuclear complex **6**. This was filtered, and when the filtrate was left to stand for several days in the open air, a new product formed, whose analysis indicated the formula $[Mn(\mu\text{-}3\text{-}ClPhCOO)_2(bpy)]_n\cdot nH_2O$. The crystals obtained were suitable for X-ray characterization. The yield was 30%. Anal. Calcd for complex **10**, $C_{24}H_{18}Cl_2MnN_2O_5$: C, 53.33; H, 3.33; N, 5.18; Cl, 13.14. Found: C, 53.3; H, 3.3; N, 5.1; Cl, 13.0. FT-IR data (KBr, main bands, cm^{-1}): 1644 (vs), 1598 (vs), 1565 (vs), 1442 (m), 1419 (m), 1394 (vs), 1071 (m), 1019 (m), 762 (vs), 735 (s), 650 (m).

$[Mn(\mu\text{-}4\text{-}ClPhCOO)_2(bpy)]_n \cdot 2nH_2O$ (11). 2,2′-bipyridine (0.16 g, 1.0 mmol) in EtOH (50 mL) was added to a solution of $[Mn(4\text{-}ClPhCOO)_2]\cdot nH_2O$ (0.40 g, 1.0 mmol) in ethanol (50 mL) with constant stirring. The solution turned yellow immediately and was stored at room temperature for 24 h. A yellow microcrystalline solid formed, which was isolated by filtration, washed in absolute ethanol and ether and dried in air. The yield was 75%. Anal. Calcd for complex **11**, $C_{24}H_{20}Cl_2MnN_2O_6$, C, 51.61; H, 3.58; N, 5.01; Cl, 12.72. Found: C, 51.6; H, 3.7; N, 5.1; Cl, 12.7. FT-IR data (KBr, main bands, cm^{-1}): 1630 (vs), 1585 (s), 1555 (s), 1445 (s), 1413 (vs), 1176 (m), 1091 (s), 1019 (s), 769 (vs), 742 (m), 532 (m).

Spectral and Magnetic Measurements. Analysis of C, H, N, and Cl were carried out by the "Serveis Científico-Tècnics" of the Universitat de Barcelona. Infrared spectra (4000−400 cm^{-1}) were recorded from KBr pellets in a Nicolet Impact 400 FT-IR spectrometer. Magnetic susceptibility measurements were performed on a MANICS-DSM8 susceptometer equipped with an Oxford Instruments liquid helium cryostat, working down to 4.2 K. Pascal's constants were used to estimate the diamagnetic corrections for each complex. EPR spectra were recorded at X-band (9.4 GHz) frequencies with a Bruker ESP-300E spectrometer from room temperature to 4 K. Both magnetic and EPR measurements were carried out at the Servei de Magnetoquímica (Universitat de Barcelona).

X-ray Diffraction Data Collection and Refinement. Complex 4. A yellow-red crystal of **4** (0.46 × 0.23 × 0.15 mm) was mounted on a Stoe AED2 four-circle diffractometer, using graphite-monochromated Mo Kα radiation (λ = 0.710 73 Å). Unit cell parameters were determined by least-squares from the $\pm\omega$ values of 27 reflections in the range $14 < \theta < 18.5°$. In all, 4635 independent reflections were measured in the range $2.23 < \theta < 25°$ at 293(2) K; 3289 reflections [$I > 2\sigma(I)$] were considered observed. Three standard reflections were measured every hour and showed a 3% intensity variation. The extinction correction was 0.033(2). No correction for absorption was made. The oxygen atoms of the perchlorate group were disordered over two possible sites. Each group of four O atoms was refined with an overall occupancy factor, final values 0.492 and 0.508. Crystallographic data are given in Table 1. The crystal structure was solved by direct methods and Fourier syntheses using the program SHELXS[40] and refined by the full-matrix least-squares method on F^2, using the program SHELXL-93.[41] The function minimized was $\Sigma w(|F_o|^2 - |F_c|^2)^2$, where $w = |\sigma^2(I) + (0.0227P)^2 + (2.61P)|^{-1}$ and $P = (|F_o|^2 + 2|F_c|^2)/3$. Complex neutral atom scattering factors were taken from *International Tables for Crystallography*, Vol. C.[42] The hydrogen atoms were included in calculated positions as riding atoms using SHELXL-93[41] default parameters, and 390 parameters were refined for 4611 reflections. Refinement converged at R(on F) 0.067, wR(on F^2) 0.120, for 3289 observed reflections. The maximun shift/esd and the mean shift/esd were −0.002 and 0.000. Maximum and minimum peaks in the final difference maps were 0.313 and −0.265 e Å^{-3}, respectively. Figure 1 was drawn using the program PLATON.[43]

Table 1. Crystallographic Data for **4** and **10**

	4	**10**
empirical formula	$C_{54}H_{42}Cl_2Mn_2N_8O_{12}$	$C_{24}H_{18}Cl_2MnN_2O_5$
fw	1175.74	540.26
temp, K	293(2)	108
space group	$P\bar{1}$ (No. 2)	$C2/c$ (No 15)
a, Å	9.1886(10)	26.376(5)
b, Å	11.6135(9)	12.404(3)
c, Å	13.595(2)	7.095(1)
α, deg	66.225(13)	90.00
β, deg	84.073(12)	96.10(3)
γ, deg	88.593(10)	90.00
V, Å^3	1320.3(2)	2308.1(1.5)
Z	1	4
λ(Mo Kα), Å	0.710 73	0.710 73
d_{cal}, g cm^{-3}	1.479	1.555
μ(Mo Kα), cm^{-1}	6.51	8.202
R[a]	0.067	0.041
wR2[b] (**4**); wR[c] (**10**)	0.120	0.050

[a] R (on F) = $\Sigma||F_o| - |F_c||/\Sigma|F_o|$. [b] wR2 (on F^2) = $[\Sigma w(|F_o|^2 - |F_c|^2)^2/\Sigma w|F_o|^4]^{1/2}$. [c] wR (on F) = $[\Sigma w(|F_o| - |F_c|)^2/\Sigma w|F_o|^2]^{1/2}$.

Complex 10. The crystals of complex **10** were light yellow, thin plates. A crystal of 0.57 × 0.18 × 0.05 mm was chosen and X-ray diffraction data were collected at 108 K with an Enraf-Nonius CAD-4 diffractometer using graphite-monochromated Mo Kα radiation (λ = 0.710 73 Å). Unit cell parameters (Table 1**)** were determined from least-squares refinement of the setting angles of 24 reflections with 2θ angles in the range 31−49°. A total of 2019 unique reflections were recorded within $2\theta < 50°$. Three reference reflections monitored throughout the data collection showed an average intensity loss of 6%. The data were corrected for Lorentz and polarization effects and for linear decay. Experimental absorption corrections based on ψ-scans of 7 reflections were carried out.[44] The intensity statistics suggested a centrosymmetric space group, thus $C2/c$ was chosen rather than Cc. The structure was solved by direct methods[45] and successive Fourier syntheses. All non-hydrogen atoms were refined anisotropically. The extinction parameter was 2.659×10^{-7}. The positions of all hydrogen atoms were revealed in a difference Fourier map. The hydrogen bonded to the water oxygen was refined isotropically, while hydrogen atoms bonded to carbon were included at calculated, idealized positions, and not refined. The final full-matrix least-squares refinements on F, minimizing $\Sigma w(|F_o| - |F_c|)^2$, including 1748 reflections with $I > 2\sigma$, adjusting 160 parameters, converged at R and R_w indices of 0.041 and 0.050. In the final difference map the residual maxima and minima were 0.57 and −0.90 e Å^{-3}. All calculations were carried out with programs in the MolEN system.[46] Neutral atomic scattering factors were used,[47] and anomalous scattering terms were included in F_{calc}.[48] Crystallographic data are given in Table 1. Complete lists of crystal parameters, atomic coordinates, anisotropic thermal parameters, intramolecular bond distances and angles, least-squares planes, torsion angles and structure factors are given in the Supporting Material.

X-ray Absorption Data Recording and Processing. The XANES (X-ray absorption near-edge structures) and EXAFS (extended X-ray absorption fine structures) data were collected at LURE (Laboratoire

(40) Sheldrick, G. M. SHELXS. *Acta Crystallogr.* **1990**, *A46*, 467.
(41) Sheldrick, G. M. *SHELXL, Program for crystal structure refinement*; University of Göttingen: Germany, 1993.
(42) *International Tables for Crystallography*; D. Reidel Publishing Co.: Dordrecht, Holland, 1994; Vol. C.
(43) Spek, A. L. PLATON. *Acta Crystallogr.* **1990**, *A46*, C34.
(44) North, A. C. T.; Phillips, D. C.; Mathews, F. S. *Acta Crystallogr., Sect. A* **1968**, *24*, 351.
(45) Main, P.; Fiske, S. J.; Hull, S. E.; Lessinger, L.; Germain, G.; DeClerq, J. P.; Woolfson, W. W. *MULTAN80, A System Of Computer Programs for the Automatic Solution of Crystal Structures from X-ray Diffraction Data*; University of York: England, 1980.
(46) *MolEN, An Interactive Structure Solution Procedure*; Enraf-Nonius: Delft, The Netherlands, 1990.
(47) (a) Cromer, D. T. and Waber, J. T. *International Tables for X-ray Crystallography*; The Kynoch Press: Birmingham, England, 1974; Vol. IV; Vol. C, Table 2.2B. (b) Cromer, D. T.; Mann, J. B. *Acta Crystallogr., Sect. A* **1968**, *24*, 321.
(48) Cromer, D. T. *International Tables for X-ray Crystallography*; The Kynoch Press: Birmingham, England, 1974; Vol. IV, Table 2.3.1.

d'Utilisation du Rayonnement Electromagnetique, Paris-Sud University, France) on a storage ring with an energy of 1.85 GeV and a mean intensity of 300−200 mA. The measurements were carried out at the manganese K edge in the transmission mode on the EXAFS III spectrometer equipped with a two-crystal monochromator (Si-311 and Si-111 for XANES and EXAFS, respectively), the entrance slit being 0.5 mm for both types of spectrum. The monochromator was left slightly out of tune to ensure harmonics rejection. Reduced-pressure, air-filled ionization chambers were used to measure the flux intensity before and after the sample. The spectra were recorded at 10 K in a helium cryostat designed for X-ray absorption spectroscopy. The XANES spectra were recorded over 150 eV step by step, every 0.25 eV with a 2 s accumulation time per point. The spectrum of a 5 μm thick manganese foil was recorded just after or before an unknown XANES spectrum to check the energy calibration, thus ensuring an energy accuracy of 0.25 eV. The EXAFS spectra were recorded in the same way over 1000−1200 eV, with 2 eV steps and 1 s accumulation time per point. The experiments were calibrated by using the 8991.1 eV peak at the top of the edge of a metallic foil of copper and verifying that the first inflection point in all the spectra of the manganese foils was 6539 eV. Each spectrum is the sum of several independent recordings added after individual inspection (two for XANES and four for EXAFS). Samples were well-pounded microcrystalline powders of a homogeneous thickness and calculated weight that were compressed between two X-ray-transparent windows. The thickness was computed to avoid saturation effects. The absorbance jump at the edge was typically 1.

The XANES and standard EXAFS data were analyzed with the "GALAAD" [49] and "EXAFS pour le MAC" [50] programs, following a well-known procedure described elsewhere.[51−53] The modeling of the outer shells was not possible in the frame of the single scattering model, and the multiple scattering/spherical wave EXAFS *ab initio* modeling FEFF[54,55] program was used. The amplitudes and phase shifts extracted from FEFF calculations were then used to fit the outer shells. Multiple scattering EXAFS contributions were included using the method described in ref 56. The FEFF calculations were performed on a RISC system/6000 running AIX 3.2.5 of the Physical Chemistry Department of the University of València.

Results and Discussion

Syntheses. In our previous paper[57] we reported that treatment of the Mn^{III} complexes $[Mn^{III}_2(\mu\text{-O})(\mu\text{-RCOO})_2(bpy)_2(H_2O)_2](NO_3)_2$, (R = 2-ClPh, 3-ClPh, 4-ClPh) with hydrogen peroxide followed by addition of $NaClO_4$ leads to formation of the dinuclear Mn^{II} complex $[Mn^{II}_2(\mu\text{-RCOO})_2(bpy)_4](ClO_4)_2$, but in the reaction without ClO_4^- two different neutral complexes were obtained. In order to improve both yield and quality of the products and thus better characterize them, since these manganese(II) products were often found as byproducts of the synthesis of the dinuclear Mn^{III} complexes, a direct procedure was studied.

In the synthesis of the dinuclear compounds, $[Mn_2(\mu\text{-RCOO})_2(bpy)_4](ClO_4)_2$ **(1−4)**, a 1:2:1 ratio of Mn^{II}/bpy/ClO_4^- was considered. The desired product was isolated in all cases except for R = 4-ClPh, where the $[Mn(\mu\text{-4-ClPhCOO})_2(bpy)]_n\cdot nH_2O$ **(11)** chain was obtained. The dinuclear complex **(3)** precipitated only in the presence of excess $NaClO_4$ in the solution. For R = 3-ClPh, when the dinuclear complex (**2**) was collected, a new product was formed later in the filtrate, which did not present the perchlorate anion and corresponded to the chain (**10**).

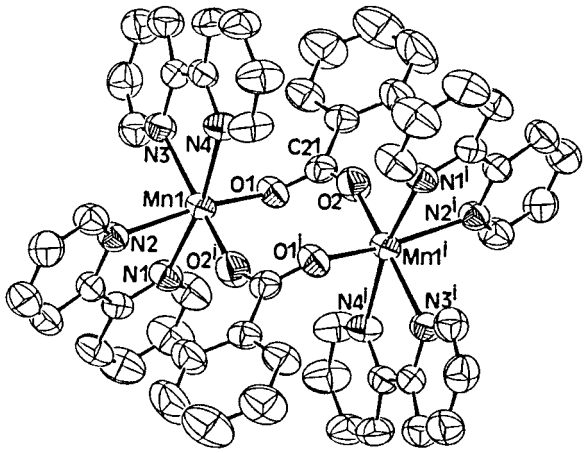

Figure 1. Drawing of the cation $[Mn_2(\mu\text{-PhCOO})_2(bpy)_4]^{2+}$ in complex (**4**) showing the *syn-anti* conformation of the carboxylate bridges. Hydrogen atoms have been omitted for clarity.

For the trinuclear compounds, in the synthetic procedure given by Shake[6] for the benzoate complex, $[Mn(PhCOO)_2]\cdot nH_2O$ and 2,2′-bipyridine (bpy) were used as starting materials; Mn^{II}/bpy ratios of $1:^2/_3$ and 1:1 were considered. However, in the synthesis of the acetate analog reported by Ménage *et al.*[58] a 1:1 ratio was used. Both ratios were followed here with the corresponding manganese(II) carboxylates, and only the trinuclear compounds $[Mn_3(\mu\text{-RCOO})_6(bpy)_2]$ with R = 2-ClPh, 3-ClPh **(5, 6)** were isolated. For R = 4-ClPh the chain **(11)** was again obtained. The analogous chain for R = 3-ClPh **(10)** was obtained after the trinuclear complex **(16)** was collected by filtration. This synthesis was repeated using 4,4′-dimethyl-2,2′-bipyridine (Me_2-bpy) instead of bpy, and the trinuclear complex was isolated in all cases, even for the 4-chlorobenzoate (**7−9**). For this series, formation of the corresponding chain was not observed.

Description of Crystal Structure of $[Mn_2(\mu\text{-PhCOO})_2(bpy)_4](ClO_4)_2$ (4). The structure of $[Mn_2(\mu\text{-PhCOO})_2(bpy)_4](ClO_4)_2$ (**4**)[59] is depicted in Figure 1. Selected bond lengths and angles are listed in Table 2. The molecule contains a crystallographic inversion center, relating both halves of the dinuclear unit. The perchlorate anions are disordered. Manganese ions are bridged by two μ-benzoate groups in a *syn-anti* fashion, that is, the lone pair on the carboxylate oxygens are opposite each other. Six-coordination on each manganese ion is completed by two chelating bpy groups; the geometry at each metal center is distorted octahedral. The bond lengths from the oxygen of the carboxylate (average d_{Mn-O} = 2.128 Å) are shorter than distances to the nitrogens (average d_{Mn-N} = 2.273 Å). Further, the distances from the N *trans* to the oxygen of the carboxylate are slightly larger (2.279, 2.292 Å) than those from the N *cis* to the oxygen (2.258, 2.265 Å), probably caused by the shorter Mn−O distances. The nonbonding interatomic Mn···Mn distance is 4.509 Å, similar to Mn···Mn distances found in analogous complexes in which carboxylate groups also

(49) Noinville, V.; Michalowicz, A. *GALAAD*; Société Française de Chimie: Paris, 1991; pp 116−117.
(50) Michalowicz, M. *EXAFS pour le MAC*; Société Française de Chimie: Paris, 1991; pp 102−103.
(51) Teo, B. K. *EXAFS: basic Principles and Data Analysis*; Springer-Verlag: Berlin, 1986; Vol. 9.
(52) Königsberger, D. C.; Prins, R. *X-Ray Absorption Principles, Applications, Techniques of EXAFS, SEXAFS and XANES*; Wiley: New York, 1988.
(53) Real, J. A.; Castro, I.; Bousseksou, A.; Verdaguer, M.; Burriel, R.; Castro, M.; Linares, J.; Varret, F. *Inorg. Chem.* **1997**, *36*, 455−464.
(54) Rehr, J. J.; Zabinsky, S. I.; Albers, R. C. *Phys. Rev. Lett.* **1992**, *69*, 3397.
(55) Rehr, J. J. *Jpn. J. Appl. Phys.* **1993**, *32*, 8.
(56) Michalowicz, A.; Moscovici, J.; Ducourant, B.; Cracco, D.; Kahn, O. *Chem. Mat.* **1995**, *7*, 1833−1842.
(57) Albela, B.; Corbella, M.; Ribas, J. *Polyhedron* **1996**, *15*, 91.
(58) Ménage, S.; Vitols, S. E.; Bergerat, P.; Codjovi, E.; Kahn, O.; Girerd, J. J.; Guillot, M.; Solans, X.; Calvet, T. *Inorg. Chem.* **1991**, *30*, 2666.
(59) Stoeckli-Evans, H. Institut de Chimie, Université de Neuchâtel, Switzerland.

Table 2. Selected Interatomic Distances (Å) and Angles (deg) for Complex $[Mn_2(\mu\text{-PhCOO})_4(bpy)_2](ClO_4)_2$ (**4**) with Estimated Standard Deviations (Esd's) in Parentheses

Mn(1)−Mn(1) (*i*)[a]	4.509(2)	N(1)−Mn(1)	2.258(4)
N(2)−Mn(1)	2.279(4)	N(3)−Mn(1)	2.292(4)
N(4)−Mn(1)	2.265(4)	O(1)−Mn(1)	2.139(4)
O(2)−Mn(1)	2.118(4)	C(21)−O(2)	1.242(6)
C(21)−O(1)	1.257(6)		
N(1)−Mn(1)−N(2)	72.5(2)	N(1)−Mn(1)−N(4)	168.7(2)
N(1)−Mn(1)−N(3)	97.3(2)	N(2)−Mn(1)−N(3)	93.1(2)
N(4)−Mn(1)−N(2)	103.5(2)	N(4)−Mn(1)−N(3)	72.1(2)
O(1)−Mn(1)−N(1)	89.4(2)	O(1)−Mn(1)−N(2)	161.39(14)
O(1)−Mn(1)−N(3)	84.7(2)	O(1)−Mn(1)−N(4)	93.4(2)
O(2)−Mn(1)−N(1)	92.6(2)	O(2)−Mn(1)−N(2)	82.2(2)
O(2)−Mn(1)−N(3)	167.2(2)	O(2)−Mn(1)−N(4)	97.4(2)
O(2)−Mn(1)−O(1)	103.6(2)		

[a] Symmetry transformation used to generate equivalent atoms: (*i*) $-x + 2, -y, -z + 1$.

bridge in a *syn-anti* manner: $[Mn_2(\mu\text{-MeCOO})_2(bpy)_4](ClO_4)_2$ (4.583 Å)[2,6]; $[Mn_2(\mu\text{-MeCOO})_2(L)_2](ClO_4)_2$, L = *N*,*N*′-dimethyl-*N*,*N*′-bis(2-pyridylmethyl)ethane-1,2-diamine (4.298 Å)[8]; $[Mn_2(\mu\text{-MeCOO})_2(tpa)_2](TCNQ)_2\cdot 2MeCN$, tpa = tris(2-pyridylmethyl)-amine, TCNQ = tetracyanoquinodimethane (4.145 Å).[7]

X-ray Absortion Studies of $[Mn_2(\mu\text{-3-ClPhCOO})_2(bpy)_4](ClO_4)_2$ (2). Attempts to obtain X-ray-quality crystals failed for all other dinuclear complexes of this series with $ClPhCOO^-$ as a ligand **(1**−**3)**. Therefore, we decided to study the XANES and EXAFS spectra of one of them (**2**) as a representative example of this family of compounds in order to confirm that they have the same structure as compound **4**. In fact, the use of X-ray absorption techniques in this structural area is not new and they have been previously revelead as very useful tool in coordination chemistry.[53,60−63] The normalized XANES spectrum for complex **2** is shown in Figure 2a. The intensity and energy of the K edge are typical of a Mn^{II} ion in an octahedral surrounding,[64] and the features at the top of the edge clearly indicate a distorted compressed octahedral geometry.[65] On the other hand, the small shoulder observed at *ca*. 55 eV from the pre-edge, which may be assigned to bielectronic transitions,[66] is also typical of Mn^{II} compounds. The Fourier transform of the experimental EXAFS spectrum is shown in Figure 3a. Each atomic shell surrounding the metal ion is represented by a peak on the Fourier transform. In this case, the Fourier transform comprised four main peaks: the first one corresponded to the four nitrogen atoms from two bpy and two oxygen atoms from the carboxylates; the second and third peaks included essentially the remaining carbon atoms of the amines and carboxylates; and the last feature was tentatively assigned to the intramolecular Mn···Mn distance as the major contribution.

A complete quantitative discussion of the local structure around the metal ions including atoms in a sphere of 5 Å is impossible in the frame of the single scattering approach of the standard EXAFS formula, due to the multiple scattering. That being so, a FEFF calculation using $[Mn_2(\mu\text{-PhCOO})_2(bpy)_4](ClO_4)_2$ **(4)** as a model compound was carried out. The complete set of Cartesian coordinates was used for these calculations. The FEFF model was compared with the experimental data (Figure 3b) and showed good agreement, which confirmed that the structure of the two compounds is similar. A quantitative analysis of the first shell and the Mn···Mn intramolecular distance was then performed for complex **2** by using the amplitudes and phase shifts extracted from the FEFF calculation. The resulting average distances from the Mn were as follows: two O atoms at 2.18 Å, four N atoms at 2.28 Å, and one Mn at 4.6 Å. Least-squares refinement resulted in the fit shown in Figure S1 (Supporting Information), and the computed results are listed in Table S1. These distances were similar to those of complex **4** (average Mn−O = 2.13 Å, average Mn−N = 2.27 Å, Mn···Mn = 4.509 Å), although the Mn−O and Mn−Mn distances were somewhat larger, possibly due to the effect of the chloro-substituent.

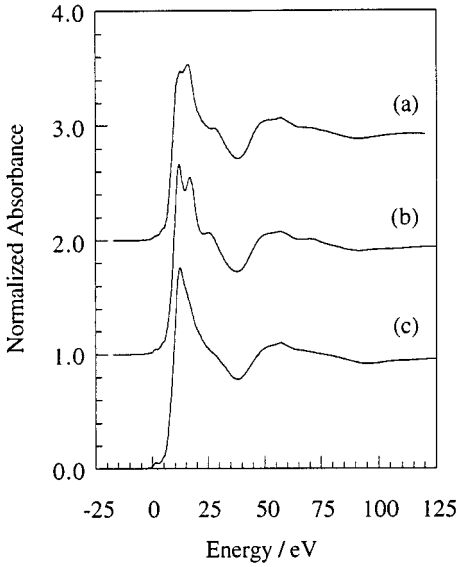

Figure 2. Normalized XANES spectra at the manganese K edge at 10 K for (a) $[Mn_2(\mu\text{-3-ClPhCOO})_2(bpy)_4](ClO_4)_2$ (**2**), (b) $[Mn(\mu\text{-4-ClPhCOO})_2(bpy)]_n\cdot nH_2O$, (**11**), and (c) $[Mn_3(\mu\text{-3-ClPhCOO})_6(bpy)_2]$ (**6**).

Because all complexes presented similar magnetic properties (see below), the same structure, *i.e.* $[Mn_2(\mu\text{-RCOO})_2(bpy)_4](ClO_4)_2$, might be proposed for all the chloro-derivative complexes. Besides, the analyses and IR data were in good agreement with this formula.

Description of Crystal Structure of $[Mn(\mu\text{-3-ClPhCOO})_2(bpy)]_n\cdot nH_2O$ (10).[67] The structure consists of an infinite chain, as shown in Figure 4. Bond lengths and angles are gathered in Table 3. The manganese atom is located on a 2-fold axis and presents a distorted octahedral coordination sphere, which consists of the two N atoms of a bipyridine (bpy) ligand (d_{Mn-N} = 2.277 Å) and four carboxylates, two *trans* to each other and *cis* to the N of the bpy ($d_{Mn-O(1)}$ = 2.196 Å) and two *cis* to each other and *trans* to the N of the amine ($d_{Mn-O(2)}$ = 2.104 Å). The Mn−O distance for the carboxylates *trans* to the amine are shorter, due probably to the larger Mn−N bond, as was observed for the dinuclear compound. The 3-chlorobenzoate ligands bridge centrosymmetrically related manganese atoms.

(60) Gadet, V.; Mallah, T.; Castro, I.; Verdaguer, M. *J. Am. Chem. Soc.* **1992**, *114*, 9213.
(61) Lloret, F.; Ruiz, R.; Julve, M.; Faus, J.; Journaux, Y.; Castro, I. *Chem. Mat.* **1992**, *4*, 1150.
(62) Lloret, F.; Ruiz, R.; Cervera, B.; Castro, I.; Julve, M.; Faus, J.; Real, J. A.; Sapiña, F.; Journaux, Y.; Colin, J. C. *J. Chem. Soc., Chem. Commun.* **1994**, 2615.
(63) Ruiz, R.; Surville- Barland, C.; Journaux, Y.; Colin, J. C.; Castro, I.; Cervera, B.; Julve, M.; Lloret, F.; Sapiña, F. *Chem. Mater.* **1997**, *9*, 201−209.
(64) Nakatani, K.; Carriat, J. Y.; Journaux, Y.; Kahn, O.; Lloret, F.; Renard, J. P.; Pei, Y.; Sletten, J.; Verdaguer, M. *J. Am. Chem. Soc.* **1989**, *111*, 5739.
(65) Cartier, C.; Verdaguer, M.; Menage, S.; Girerd, J. J.; Tuchagues, J. P.; Mabad, B. *J. Phys.* **1986**, *47*, 623−625.
(66) Cartier, C. Ph.D. Thesis, Centre Universitaire Paris-Sud, Orsay, France, 1988.
(67) This structure was solved by J. Sletten, Department of Chemistry, University of Bergen, Norway.

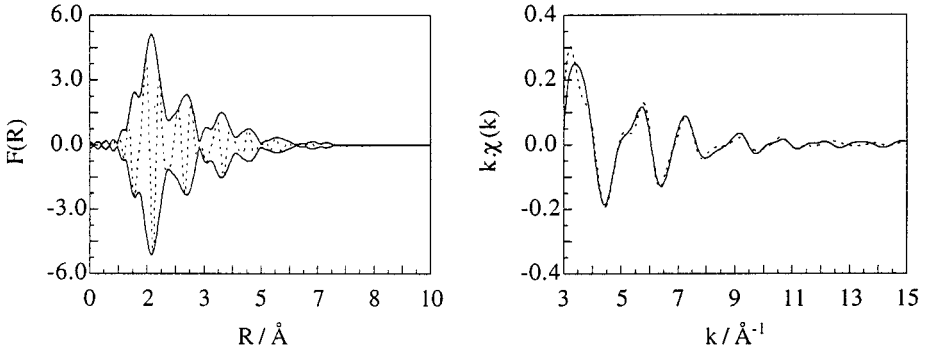

Figure 3. Fourier transform of the experimental EXAFS spectrum (left) and comparison of the experimental (dashed line) and calculated (solid line) *k* space EXAFS spectra (right) for $[Mn_2(\mu\text{-}3\text{-}ClPhCOO)_2(bpy)_4](ClO_4)_2$ (**2**) using the FEFF method on the model compound $[Mn_2(\mu\text{-}PhCOO)_2(bpy)_4](ClO_4)_2$ (**4**) at the manganese K edge.

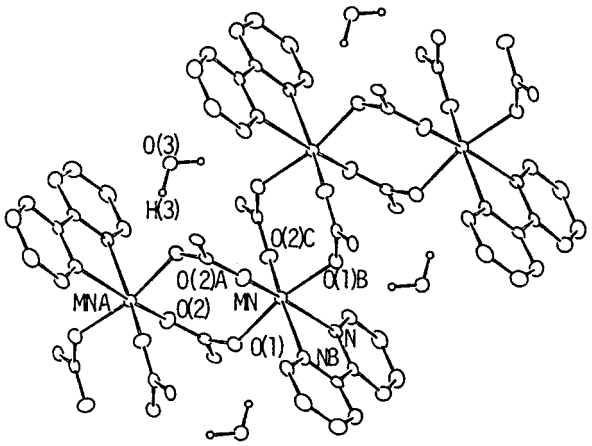

Figure 4. Plot of the one-dimensional complex $[Mn(\mu\text{-}3\text{-}ClPhCOO)_2(bpy)]_n{\cdot}nH_2O$, (**10**). The benzenic rings of the μ-3-ClPhCOO$^-$ groups are omitted for clarity.

Table 3. Main bond Distances (Å) and Angles (deg) for $[Mn(\mu\text{-}3\text{-}ClPhCOO)_2(bpy)]_n{\cdot}nH_2O$ (**10**) with Estimated Standard Deviations (Esd's) in Parentheses[a]

Mn−MnA	4.515(1)	Mn−O(1)	2.196(2)
Mn−O(2)	2.104(2)	Mn−N	2.277(2)
O(1)−C(7)	1.260(3)	O(2)−C(7)	1.261(3)
O(1)−Mn−O(1)B	168.88(6)	O(2)A−Mn−O(2)C	111.77(7)
N−Mn−NB	71.27(7)	O(1)−Mn−O(2)A	100.52(6)
O(1)−Mn−N	87.05(6)	O(1)−Mn−O(2)C	85.76(6)
O(1)−Mn−NB	83.92(6)	O(2)A−Mn−N	158.16(7)
O(2)A−Mn−NB	89.05(7)		

[a] Symmetry codes: A = 1 − *x*, −*y*, −*z*; B = 1 − *x*, *y*, $^1/_2$ − *z*; C = *x*, −*y*, *z* + $^1/_2$.

In this way, infinite zigzag chains consisting of doubly carboxylate-bridged manganese atoms are formed (Figure 4). The Mn···Mn distance within the chain is 4.515 Å. This value is comparable with the d_{Mn-Mn} of 4.509 Å in the former complex, $[Mn_2(\mu\text{-}PhCOO)_2(bpy)_4](ClO_4)_2$ **(4)**, as expected since in the chain the two carboxylate bridges also present a *syn-anti* conformation. Indeed, the structure of the dinuclear complex is observed within the chain, which might be considered as a polymer of "$Mn(\mu\text{-}RCOO)_2Mn$" units bridged by two μ-carboxylates. So, such similarity between both structures might explain the finding that, when we attempted to synthesize the dinuclear complex $[Mn_2(\mu\text{-}RCOO)_2(bpy)_4](ClO_4)_2$, the $[Mn(\mu\text{-}RCOO)_2(bpy)]_n{\cdot}nH_2O$ chain was also isolated in some cases. Besides, the water of crystallization, which is situated on a 2-fold axis, is hydrogen-bonded to two carboxylate O(1) atoms of alternate manganese ions within the same chain ($d_{O(1)-H}$ = 1.957 Å, $d_{O(1)-O(3)}$ = 2.864 Å, O(3)−H(3)···O(1) = 153°), thus stabilizing the zigzag chain structure. A similar zigzag arrangement has recently been described for $[Mn(\mu\text{-}Cl)_2(bpy)]_n$,[68] where the chloride ions occupy the position of the carboxylates in the chain studied here. Furthermore, the hydrogen bond with the O(1) of the carboxylate may cause the Mn−O(1) distance to be slightly larger than that with the O(2), which is not hydrogen-bonded to the water molecule, and the octahedral environment of the metal becomes distorted.

X-ray Absorption Studies of $[Mn(\mu\text{-}4\text{-}ClPhCOO)_2(bpy)]_n{\cdot}nH_2O$ (11). In the absence of the crystal structure for the complex with 4-ClPhCOO$^-$ as carboxylate **(11)**, XANES and EXAFS spectroscopies were used to characterize it structurally. The XANES spectrum for **11** is shown in Figure 2b. The intensity and energy of the K edge is similar to the dinuclear manganese(II) complex **2** and the shoulder at *ca*. 55 eV from the pre-edge also appears. The top of the edge is structured, and the shape suggests that the local environment of Mn^{II} metal ion is octahedral elongated.[65] As in compound **2**, four main peaks are observed in the experimental Fourier transform (Figure 5a): the first one corresponds to the first coordination sphere of the metal, the second and third peaks include mainly the remaining carbon atoms of the ligands, and the fourth one might be tentatively assigned to distances to the closest Mn as the greater contribution. Only the distance with the first Mn was tentatively assigned, since a second Mn may be located quite far from the absorber atom to have a considerable contribution in the spectrum. A FEFF calculation for complex $[Mn(\mu\text{-}3\text{-}ClPhCOO)_2(bpy)]_n{\cdot}nH_2O$ (**10**) was performed, using the complete set of Cartesian coordinates. The superimposability of the spectrum calculated for this compound and the experimental one of **11** indicates the good quality of the model considered (Figure 5b). The amplitudes and phase shifts deduced from the FEFF calculation were used to fit the experimental data of complex **11** (4-ClPh). The resulting average distances were the following: Mn−O = 2.14 Å, Mn−O = 2.20 Å, Mn−N = 2.30 Å, and Mn···Mn = 4.6 Å, which are similar to those of $[Mn(\mu\text{-}3\text{-}ClPhCOO)_2(bpy)]_n{\cdot}nH_2O$ (**10**) (Table 3). Least-squares refinement resulted in the fitting shown in Figure S1 (Supporting Information), and the computed results are listed in Table S1.

X-ray Absortion Studies of $[Mn_3(\mu\text{-}3\text{-}ClPhCOO)_6(L)_2]$, L = bpy, Me_2-bpy (6, 8). In the absence of crystal structure of any trinuclear compound (**5**−**9**), a formula $[Mn_3(\mu\text{-}RCOO)_6(L)_2]$ was proposed on the basis of the analyses, IR data, and the study of the magnetic properties (see below). This structure was confirmed by the analysis of the XANES and EXAFS spectra at the Mn K edge. Two of these complexes were

(68) Lubben, M.; Meetsma, A.; Feringa, B. L. *Inorg. Chim. Acta* **1995**, *230*, 169.

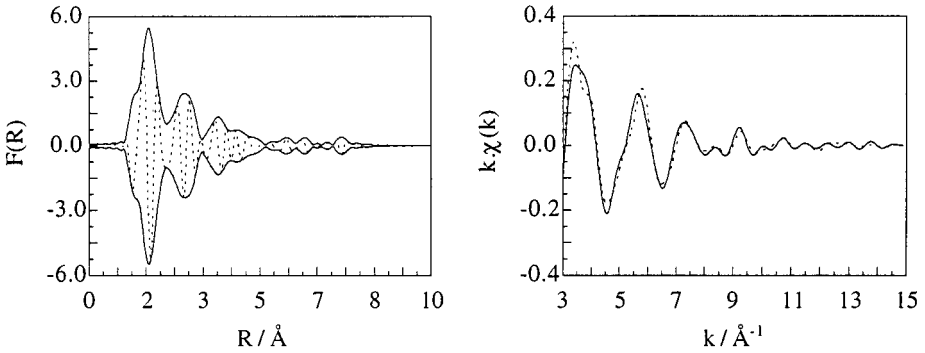

Figure 5. Fourier transform of the experimental EXAFS spectrum (left) and comparison of the experimental (dashed line) and calculated (solid line) *k* space EXAFS spectra (right) for $[Mn(\mu\text{-}4\text{-}ClPhCOO)_2(bpy)]_n \cdot nH_2O$ (**11**) using the FEFF method on the model compound $[Mn(\mu\text{-}3\text{-}ClPhCOO)_2(bpy)]_n \cdot nH_2O$ (**10**) at the manganese K edge.

Chart 1

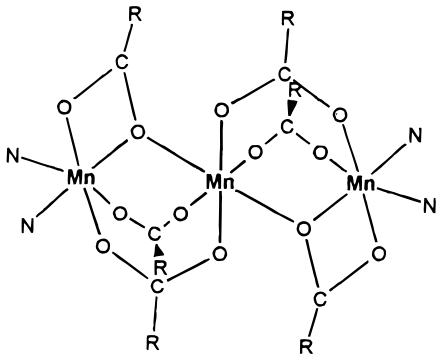

selected as representative compounds for such studies: one of the bpy series, complex **6**, and the corresponding complex of the Me_2-bpy series with the same carboxylate (**8**). The analog with benzoate as a bridge $[Mn_3(\mu\text{-}PhCOO)_6(bpy)_2]$ described elsewhere[6] was considered as a model. This structure consists of a linear array, in which each pair of Mn atoms is bridged by three carboxylates, showing two types of bonding mode. Two of the benzoates bridge symmetrically in a *syn-syn* bidentate fashion, whereas the third is described as "asymmetrical", with one carboxylate oxygen bridging the two metals and the second bound to the terminal manganese atom. The central ion thus exhibits an octahedral coordination sphere made of six oxygen atoms from six different benzoate groups, while the terminal ions present a distorted octahedral environment of four oxygen atoms and two nitrogen atoms that come from a bpy molecule (see Chart 1). The bridging mode found in this compound is quite rare among carboxylate bridged complexes.

The XANES spectrum of complex **6** at the Mn K edge is shown in Figure 2c. The spectrum is typical of manganese(II) in an octahedral environment, as pointed out for the former complexes. The top of the edge was featureless, which may indicate that (i) the distortion of the octahedral environment is weak[69] or (ii) the spectrum is the result of the average contributions of two opposite distorted manganese ions, one compressed octahedral manganese and the other elongated. A comparison between the XANES spectra of **6** and **8** (Figure S2) reveals that the two edges are almost superimposable, suggesting strong similarities in the geometry at the metal ion. The similarity between the experimental EXAFS spectra and the corresponding Fourier transforms for complexes **6** and **8** (Figure 6 and Figure S3) also suggests that the local structure of the Mn^{II} ion might be the same. In this case, only three main peaks were observed in the Fourier transforms and the last feature might be tentatively assigned to distances Mn_c-Mn_t as the larger contribution.

A FEFF calculation of the EXAFS spectrum was carried out using the crystallographic coordinates of the benzoate analogue $[Mn_3(\mu\text{-}PhCOO)_6(bpy)_2]$[6] as a theoretical model. This simulation was difficult, since the two terminal Mn and the central ion showed different contributions and average values were considered. Therefore, the EXAFS study of this system may be more complicated than that of the former dinuclear and monodimensional complexes, and only average distances may be derived. Figure 6b displays a comparison between the experimental data of complex **6** and the theoretical model. The fit of the filtered first and third main peaks of the Fourier transform, considering the parameters obtained from the FEFF calculations for this model, gave Mn−O distances between 2.09 and 2.28 Å, Mn−N distances of 2.23−2.25 Å, and a Mn···Mn distance of 3.6 Å in both cases. Least-squares refinement resulted in the fit shown in Figure S1 (Supporting Information), and the computed results are listed in Table S1. The values obtained are similar to the average of the distances around the Mn atom for the model complex $[Mn_3(\mu\text{-}PhCOO)_6(bpy)_2]$[6] ($Mn_{terminal}-O$ = 2.075, 2.098, 2.274, 2.286 Å; $Mn_{central}-O$ = 2.128, 2.170, 2.239 Å; Mn−N = 2.261, 2.268 Å; Mn_t-Mn_c = 3.588 Å), thereby confirming the proposed structure, *i.e.*, $[Mn_3(\mu\text{-}RCOO)_6(bpy)_2]$.

Magnetic Susceptibility Study. Magnetic susceptibility data were recorded for all complexes (**1**−**12**) from room temperature to 4 K. For the dinuclear complexes (**1**−**4**) the value of χ_M was 0.04 $cm^3\ mol^{-1}$ at room temperature and increased with temperature, reaching a maximum of $\chi_M T \approx 0.35-0.38\ cm^3\ mol^{-1}$ at 4−5 K, and then decreased, tending to zero at 0 K. The $\chi_M T$ product began at ≈8−9 $cm^3\ mol^{-1}$ K at *ca.* 300 K, which was close to the value for two uncoupled $S = {}^5/_2$ ions (8.75 $cm^3\ mol^{-1}$ K). The $\chi_M T$ values decreased slowly with temperature to 7.5 $cm^3\ mol^{-1}$ K at 50 K, followed by a further larger decrease, reaching a value of 1−2 $cm^3\ mol^{-1}$ K at 4 or 2 K for complex **3**. This behavior is typical for weak antiferromagnetic coupling between two Mn^{II} centers.

The spin Hamiltonian $\mathbf{H} = -J_{12}\mathbf{S}_1\mathbf{S}_2$ was used to fit the magnetic results assuming that the two Mn^{II} ions present the same *g* value. The parameters *J* and *g* obtained from least-squares fitting of the χ_M *vs* temperature data to the theoretical equation,[70] are listed in Table 4. All *J* values are similarly low. The *g* parameter presented a value close to 2.0 in all cases,

(69) Roe, A. L.; Schneider, D. J.; Mayer, R. J.; Pyrz, J. W.; Widom, J.; Que, L. J. *J. Am. Chem. Soc.* **1984**, *106*, 1676.

(70) (a) Van Vleck, J. H. *The Theory of Electric and Magnetic Susceptibilities*; Oxford University Press: London, 1932. (b) O'Connor, C. J. *Prog. Inorg. Chem.* **1982**, *29*, 238

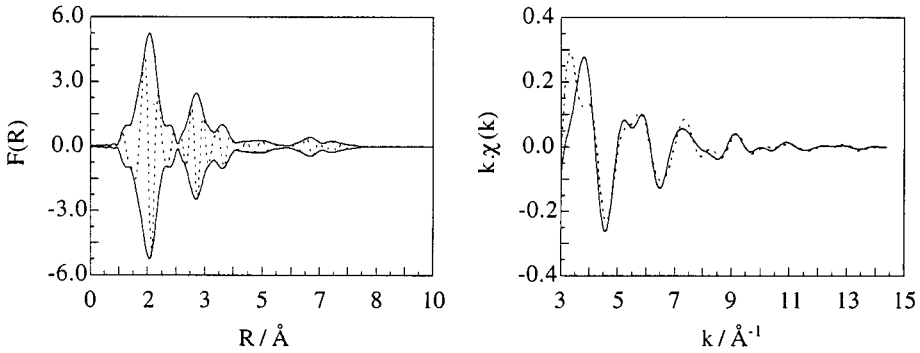

Figure 6. Fourier transform of the experimental EXAFS spectrum (left) and comparison of the experimental (dashed line) and calculated (solid line) *k* space EXAFS spectra (right) for $[Mn_3(\mu\text{-}3\text{-}ClPhCOO)_6(bpy)_2]$ **(6)** using the FEFF method on the model compound $[Mn_3(\mu\text{-}PhCOO)_6(bpy)_2]$ at the manganese K edge.

Table 4. Parameters Obtained from the Fit of the Susceptibility Data of Complexes **1**−**9**

complex	J (cm^{-1})	g	complex	J (cm^{-1})	g
1	−1.73	2.03	**6**	−3.04	2.02
2	−1.79	2.05	**7**	−3.22	2.02
3	−1.70	2.00	**8**	−3.15	2.03
4	−1.76	2.00	**9**	−2.07	2.04
5	−2.73	2.01			

which agrees with the presence of manganese(II) ions, which do not exhibit spin−orbit coupling. From the magnetic point of view, the coupling constant *J*, which reflects the manganese−manganese interactions, is determined in a first approach by the bridges between the two metal ions. It is generally assumed[14,71] that the carboxylates are ineffective in transmitting the exchange interaction. Accordingly, complexes with only carboxylate bridging ligands may exhibit small negative exchange coupling constants, as observed here. This is consistent with the great distance between the two manganese ions found in these cases. *J* values reported in the literature for manganese(II) complexes with only carboxylates as bridging ligands are always weak, between −0.2 and −5 cm^{-1} approximately.[4,5,7,11,12,31]

For the trinuclear complexes (**5**−**9**) the value of χ_M was ≈0.05 cm^3 mol^{-1} at room temperature and increased continuously with temperature. Since a maximum in the χ_M versus temperature plot was not observed, $\chi_M T$ provided the best fit to a theoretical equation. For all complexes, $\chi_M T$ at room temperature (≈12 cm^3 mol^{-1} K at 290 K) was smaller than the expected value for three Mn^{II} atoms uncoupled with $S_i = {}^5/_2$ and $g_i = 2$ each ($\chi_M T = 13.125$ cm^3 mol^{-1} K). This indicates antiferromagnetic coupling, which was confirmed by the decrease in $\chi_M T$ when *T* decreased, reaching 4.3 cm^3 mol^{-1} K at 4.2 K, which corresponds (within experimental uncertainty) to the expected value $\chi_M T = 4.375$ cm^3 mol^{-1} K for a spin state $S = {}^5/_2$ with $g = 2$ (Figure 7). Similar behavior has been reported for the acetate[26] and benzoate[6] analogues.

Taking into account the structure of these compounds, the following Kambe vector-coupling scheme (Scheme 1)[72] was considered:

The spin Hamiltonian that describes the low-lying electronic states is given by eq 1, where it is assumed that $J_{12} = J_{23} = J$.

$$\mathbf{H_S} = -J(\mathbf{S_1S_2} + \mathbf{S_2S_3}) - J_{13}\mathbf{S_1S_3} \qquad (1)$$

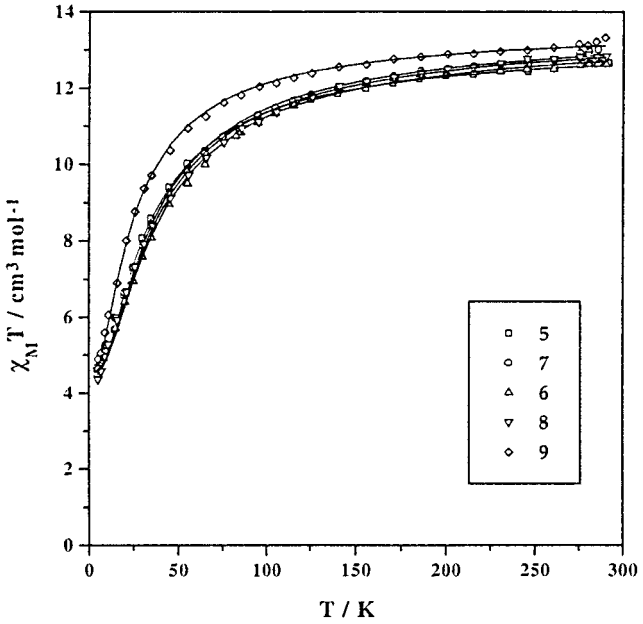

Figure 7. $\chi_M T$ *vs T* plot for $[Mn_3(\mu\text{-}RCOO)_6(L)_2]$ (R = 2-ClPh, 3-ClPh, 4-ClPh; L = bpy, Me_2-bpy) **(5**−**9)**. The solid line is the best fit to the experimental data.

Scheme 1

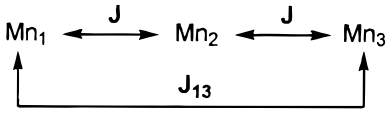

In fact, all authors fix $J_{13} = 0$ to fit the experimental susceptibility data,[26,29,73] owing to the long distance between the two terminal Mn^{II} ions and the linearity of the known structures (with acetate and benzoate).

From the Van Vleck formula,[70a] the susceptibility expression for three linear Mn^{II} (d^5) ions is obtained,[6] and this equation was incorporated into a nonlinear, least-squares computer program, which was then used to fit the experimental $\chi_M T$ versus temperature data as a function of an exchange coupling parameter *J* and an isotropic *g* value. The solid lines in Figure 7 represent the best fit obtained for each complex. The corresponding *J* and *g* values are listed in Table 4. The *J* values obtained range between −2.1 and −3.2 cm^{-1}, which are of the same order as the values found for similar complexes: $[Mn_3(\mu\text{-}MeCOO)_6(bpy)_2]$[26] ($J = -4.4$ cm^{-1}) and $[Mn_3(\mu\text{-}MeCOO)_6$-

(71) Hartman. J. A. R.; Rardin, R. L.; Chaudhuri, P.; Pohl, K.; Wieghardt, K.; Nuber, B.; Weiss, J.; Papaefthymiou, G. C. *J. Am. Chem. Soc.* **1987**, *109*, 7387.
(72) Kambe, K. *J. Phys. Soc. Jpn.* **1950**, *5*, 48.
(73) Baldwin, M. J.; Kampf, J. W.; Kirk, M. L.; Pecoraro, V. L. *Inorg. Chem.* **1995**, *34*, 5252.

$(L)_2]$, L = BIPhMe[29] ($J = -5.6$ cm^{-1}). This indicates that weak antiferromagnetic coupling is mediated by the bridging carboxylate in these complexes, which is as expected, since the Mn−O distances are relatively long in such compounds.[26,29] The coupling is even weaker than the exchange observed for hydroxide- and alkoxide-bridged species,[29] as seen for the dinuclear Mn^{II} compounds. As pointed out by Baldwin *et al*.,[73] it does not appear that the different carboxylate bridging modes have a significant effect on the magnetic coupling in these systems. The J values obtained lead to an $(S_{13},S_T) = (5, {}^5/_2)$ spin ground state, which is energetically separated from the $(4, {}^3/_2)$ and $(5, {}^7/_2)$ lowest excited states by ${}^5/_2J$ and ${}^7/_2J$, respectively.[26,66] As the J values are quite small, the first excited states may lie close to the ground state, and at room temperature many states may be populated.

For complexes **10** and **11** the value of χ_M was ≈0.025 cm^3 mol^{-1} at room temperature, and increased continuously with temperature (Figure 8) giving a maximum close to 10 K for **10** and at *ca*. 4 K for **11**. $\chi_M T$ values decreased monotonically from ≈4.5 cm^3 mol^{-1} K at 290 K (a typical value for an $S = {}^5/_2$ ion, assuming $g = 2.0$). The shape of the two curves clearly indicates that complex **10** showed greater antiferromagnetic coupling than **11**.

As reported in the literature for similar one-dimensional manganese(II) complexes,[74] the magnetic susceptibility data for complexes **10** and **11** may be analyzed according to two isotropic Heisenberg models for linear chains: (a) the scaling model of Wagner and Friedberg[32] with $S = {}^5/_2$ and (b) the Weng model[75] with coefficients generated by Hiller *et al*.[76] for $S = {}^5/_2$.

The isotropic Heisenberg Hamiltonian considered in both cases was

$$\mathbf{H} = -J \Sigma \mathbf{S}_i \mathbf{S}_j$$

According to the Wagner and Friedberg model (a), the molar magnetic susceptibility is given by

$$\chi_M = \frac{Ng^2\beta^2 S(S+1)}{3kT} \times \frac{(1+U)}{(1-U)}$$

where $U = \coth K - 1/K$ and $K = JS(S+1)/kT$.

According to the second model (b),

$$\chi_M = \frac{Ng^2\beta^2}{kT} \times \frac{(A+BX^2)}{(1+CX+DX^3)}$$

where $A = 2.9167$, $B = 208.04$, $C = 15.543$, $D = 2707.2$, and $X = |J|/2kT$.

Experimental magnetic susceptibility data were analyzed using both models. Dotted and solid lines in Figure 8 represents the best fits to the Wagner−Friedberg and Weng−Hiller models respectively. Similar J and g values were obtained in both fits, and an average value was considered as a final parameter in each case (Table 5). However, the Weng−Hiller model gave better agreement. In fact, the main feature was the low values of J, in accordance with the presence of only bridging carboxylates.

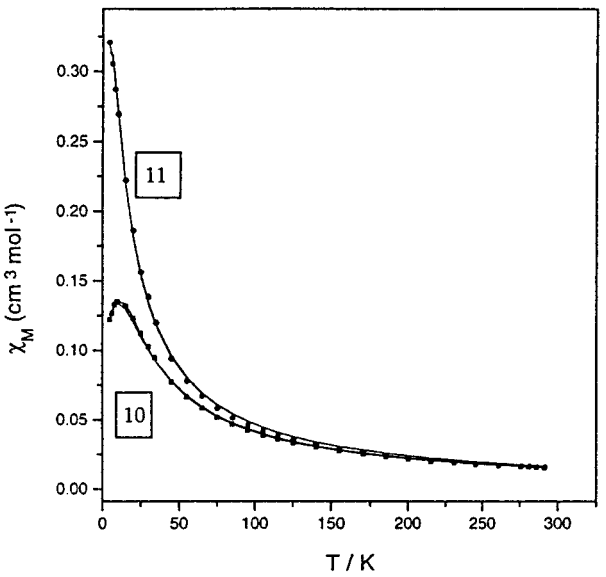

Figure 8. χ_M *vs* temperature plot for (A) $[Mn(\mu\text{-}3\text{-}ClPhCOO)_2(bpy)]_n \cdot nH_2O$ (**10**) and (B) $[Mn(\mu\text{-}4\text{-}ClPhCOO)_2(bpy)]_n \cdot nH_2O$ (**11**). The dotted and solid lines are the best fit to the experimental data using the Wagner−Friedberg and Weng−Hiller models, respectively.

Table 5. Parameters Obtained from the Fit of the Susceptibility Data of Complexes **10** and **11**

	Wagner-Friedberg Model		Weng−Hiller Model	
complex	J (cm^{-1})	g	J (cm^{-1})	g
10	−1.72	2.05	−1.58	2.05
11	−0.74	2.1	−0.72	2.1

EPR Spectra. The three families of manganese(II) compounds studied show weak Mn···Mn interactions, so even at low temperatures a number of spin states may be populated. This may lead to many possible transitions and thus a complicated EPR spectrum. At room temperature all the complexes showed a signal centered at g ∼ 2, which was quite broad in general. However, at 4 K the spectrum of each type of compound was quite different, which allowed us to identify each kind of complex.

The spectrum at 4 K for the dinuclear complexes **(1−4)** presented a broad signal centered at $g \sim 2$, which was flanked by one feature at ∼2800 G and another at ∼4200 G. Other less intense signals were observed at lower field (Figure 9A). The spin of the ground state for these compounds is $S = 0$. Therefore, at 4 K they should be EPR-silent. However, in our case, as the J value is so small ($J \sim -1.7$ cm^{-1}), the lowest excited states may also be populated besides the $S = 0$ ground state. As described by Adams *et al*.[5] for weakly coupled dinuclear complexes, the features observed probably correspond to the superposition of the spectra of various excited spin states ($S = 1-5$) of the manganese(II) pair, modulated by a Boltzmann distribution, since more states may contribute due to the small J values.

For the trinuclear complexes **(5−9)** the intensity of the signal at $g \sim 2$ observed at room temperature decreased with the temperature. At 4 K the spectrum became quite complicated: it showed intense signals at low field and other less intense signals, at high field (Figure 9B). These systems present an $S_T = {}^5/_2$ ground state. At 4 K this spin state may be populated, which can exhibit zero-field splitting (ZFS). If the ZFS effects were negligible, *i.e.*, $|J| > |A|$ (A is the hyperfine splitting parameter), a narrow signal may arise around $g = 2$.[26,77] However, if the ZFS is considerable, this signal should be split

(74) Betz, P.; Bino, A.; Du, J.-L.; Lo, I. S.-M.; Thompson, R. C. *Inorg. Chim. Acta* **1990**, *170*, 45.
(75) Weng, C. H. Ph.D. Dissertation, Carnegie-Mellon University, Pittsburgh, PA, 1968.
(76) Hiller, W.; Strahle, J.; Dtaz, A.; Hanack, M.; Hatfield, W. E., terHaar, L. W.; Gutlich, P. *J. Am. Chem. Soc*. **1984**, *106*, 329.

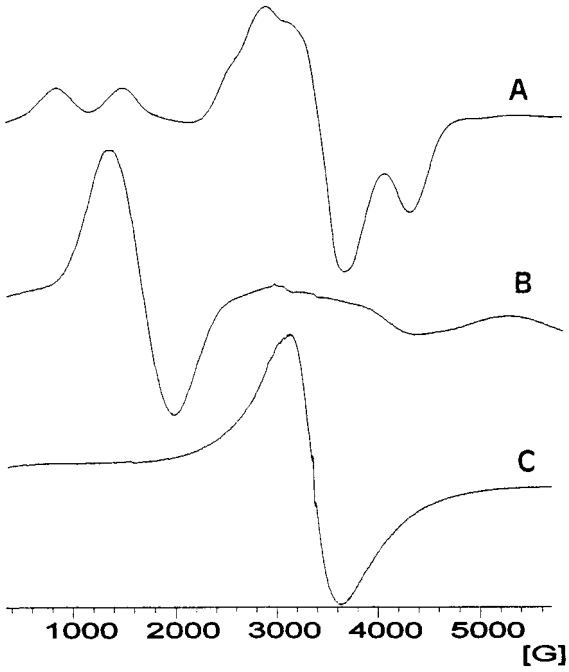

Figure 9. Comparative X-band EPR spectra of a microcrystalline sample at 4 K of complexes (A) $[Mn_2(\mu\text{-}3\text{-}ClPhCOO)_2(bpy)_4](ClO_4)_2$ (**2**), (B) $[Mn_3(\mu\text{-}3\text{-}ClPhCOO)_6(bpy)_2]$ (**6**), and (C) $[Mn(\mu\text{-}3\text{-}ClPhCOO)_2(bpy)]_n \cdot n\ H_2O$ (**10**).

into several features, and thus signals at low field may be observed, as found here. No quantitative explanation of these low-temperature features has been reported so far. Nevertheless, these spectra at 4 K are similar to that reported by Ménage *et al.*[26] for the acetate analogue at 10 K. On the other hand, complex **8** showed a narrow band at $g \sim 2$ at room temperature, in contrast to the broad features presented by the other complexes of the series. The narrowing of this signal might be due to intermolecular interactions between the molecules, as will be discussed for the manganese(II) chains (see below).

The EPR spectrum for the chains (**10**, **11**) presented a single band centered at g ~ 2 at room temperature, which was narrow for **10** (~100 G) and quite broad for **11** (~500 G). Complex **11** also showed a broad shoulder at 2200−2300 gauss. A broad feature at $g \sim 2$ (~700 G) was observed at 4 K in both cases (Figure 9C).

EPR spectra of one-dimensional systems are difficult to interpret, even from a qualitative point of view. In fact, as pointed out by Gatteschi and Bencini,[78] the effect of the dipolar interaction is great in these cases, leading to a broadening of the main line of the spectrum. The addition of one more spin to a cluster yields an increasing number of transitions, only some of which are centred at ν_o, the rest flanking it at different distances. The result is a homogeneous broadening of the line. On the other hand, when isotropic exchange is also present the exchange interaction yields a number of levels, which increases with the number of interacting spins. As long as the various multiplets are not split in zero field, the resonance may be centered at ν_o, and no shift or broadening may occur. In other words, the $\mathbf{H}_{exchange}$ Hamiltonian may not affect the spectrum, while the $\mathbf{H}_{dipolar}$ Hamiltonian may yield broadening. If $\mathbf{H}_{dip} \gg \mathbf{H}_{ex}$, the broadening effect dominates; in contrast, if $\mathbf{H}_{dip} \ll \mathbf{H}_{ex}$, then a completely new situation arises, in which the signals are narrow, and the line widths often become comparable to those of the individual spins embedded in the magnetic lattice: this regime is referred to as *exchange narrowing*.[75] In this theory it is necessary to take into account the relaxation time: the absorption line is centered at ν_o and is broadened by $\nu_1(t)$, the time-dependent perturbation, which is dipolar in nature; in other words, the resonance at ν_o is modulated by $\nu_1(t)$. On the other hand, it is possible to demonstrate that the *exchange narrowing* is greater in 3D > 2D > 1D systems. In isolated one-dimensional systems, the lines are broader than in three-dimensional systems. The possible effect of weak *interchain* coupling (J') may then be strong: J' yields more "three-dimensional" behavior (exchange narrowing).

There are additional broadening mechanisms: hyperfine coupling, anisotropic and antisymmetric exchange, **g** anisotropy, and crystal field effects. Fortunately, for Mn^{II} low-dimensional systems, only the hyperfine coupling and the crystal field effects are considerable. Finally, for $S > {}^1/_2$ (such as the Mn^{II} ions, $S = {}^5/_2$) another possible broadening mechanism is caused by single-ion ZFS effects.

As pointed out above, the EPR spectra of **10** and **11** showed different behavior with temperature: for 10 a considerable variation of the signal width was observed when temperature decreased, while for 11, only a slight broadening occurred, since at room temperature the $g \sim 2$ feature was already rather broad. At this stage, it is impossible to explain the origin of this difference. The fact that complex **10** exhibited antiferromagnetic coupling greater than **11** might be related to the narrower signal that the former presented at room temperature, since the higher *J* (exchange interaction) might contribute to the *exchange narrowing* ($\mathbf{H}_{ex} \gg \mathbf{H}_{dip}$). When the temperature decreases and approaches the critical point at which three-dimensional order may be established, the dipolar interactions may become larger ($\mathbf{H}_{ex} \ll \mathbf{H}_{dip}$) and the line width may then increase quite rapidly, giving a broad feature, as observed for both compounds.

Conclusions

The three chlorobenzoato anions (*ortho*, *meta*, and *para*) are not "innocent" when forming new polynuclear Mn^{II} complexes. Working with 2,2′-bipyridine (bpy) as blocking ligand and a stoichiometric amount of sodium perchlorate for 2-Cl and 3-Cl and a large excess for 4-Cl, dinuclear cationic complexes (with ClO_4- as counter-anion) may be prepared; neutral trinuclear complexes, $[Mn_3(\mu\text{-}RCOO)_6(bpy)_2]$, only for 2-Cl and 3-Cl and, finally, unexpected one-dimensional systems, $[Mn(\mu\text{-}RCOO)_2(bpy)]_n \cdot nH_2O$, for 3-Cl and 4-Cl. Their structures have been studied by X-ray and EXAFS determination. All show only bridging carboxylate ligands and, thus, long distances between the Mn centers.

The magnetic measurements showed, irrespective of their nuclearity, antiferromagnetic Mn···Mn interaction, owing to the presence of five unpaired electrons in the d orbitals, which forms a possible pathway for the interchange coupling. This antiferromagnetism is very small due to the presence of only carboxylate bridges.

The EPR spectra of the different polynuclear compounds are difficult to interpret because, even when the spin ground state is 0, they have low-lying excited states that are EPR-active, which causes the formation of wide bands at low field.

Acknowledgment. This work was supported by The Spanish Goverment (DGICYT), Grants PB93/0772 (to J.R.) and PB94-1002 (to I.C.), and The Swiss National Science Foundation, Grant 20.45315.95 (to H.S.). B.A. received an FPI Grant from

(77) Luneau, D.; Savariault, J. M.; Tuchagues, J. P. *Inorg. Chem.* **1988**, *27*, 3912.
(78) Bencini, A.; Gatteschi, D. *EPR of Exchange Coupled Systems*; Springer-Verlag: Berlin, 1990.

the Spanish Government. We also express our gratitude to Dr. F. Villain for the help in the use of the EXAFS 3 spectrometer and cryogen device and to Dr. N. Clos for recording the magnetic and EPR data.

Supporting Information Available: Tables of fractional atomic coordinates, bond distances and angles, anisotropic thermal parameters for **4** and **10**; figures showing the fitting of the EXAFS experimental data for compounds **2**, **11**, **6**, and **8** using the parameters extracted from the FEFF calculation (Figure S1), the comparison between the XANES spectra of **6** and **8** (Figure S2), Fourier transform of the experimental EXAFS spectrum and comparison of the experimental and calculated *k*-space EXAFS spectra for **8** using the FEFF method on the model compound $[Mn_3(\mu\text{-PhCOO})_6(bpy)_2]$ (Figure S3), and a table containing other parameters resulting from quantitative analyses of EXAFS data (22 pages). Ordering information is given on any current masthead page.

IC970935P